ENERGY MEASUREMENT OF PION BEAMS

by

Takenori Suzuki

M.Sc., Tokyo University, 1970

A THESIS SUBMITTED IN PARTIAL FULLFILMENT OF
THE REQUIREMENTS FOR THE DEGREE OF
MASTER OF SCIENCE

in the Department
of
Physics

We accept this thesis as conforming to the
required standard

The University of British Columbia
October, 1976

In presenting this thesis in partial fulfilment of the requirements for an advanced degree at the University of British Columbia, I agree that the Library shall make it freely available for reference and study. I further agree that permission for extensive copying of this thesis for scholarly purposes may be granted by the Head of my Department or by his representatives. It is understood that copying or publication of this thesis for financial gain shall not be allowed without my written permission.

Department of Physics

The University of British Columbia
2075 Wesbrook Place
Vancouver, Canada
V6T 1W5

Date October 6, 1976

Abstract

Pion energies between 30 MeV and 60 MeV have been determined by three methods: magnetic field, range and time of flight. The pion energy was measured to an accuracy 2 % by range and 5 % by the time of flight, and the three methods were consistant with one another. The pions which were used were produced by 500 MeV protons from the TRIUMF cyclotron. The pions were focussed into a beam using the M9 (or stopped π/μ) channel. The bending magnets of this channel define the momentum of the beam particles and thus give one method of determining the pion energy.

Differential and integral range curves for aluminum and copper were taken and the differential curves were used to determine the range. In taking the differential curve the effect of stopping plates was examined.

In the time of flight method, the leading edge type discriminator was found to give a time walk, due to the different energy-loss of particles in the plastic scintillator. This has a serious effect in determining the pion energies. However, the constant fraction discriminator was found to give dependable results and the measured energies agreed reasonably well with those of the other methods.

Energy Measurement of Pion Beams

table of contents:

list of tables: page

list of figures: page

acknowledgment

I am most grateful to Professor D.F. Measday for his very patient explanations to a novice in the field, and for his advice on this thesis. I would like to thank members of TINA group, Drs. M. Hasinoff, M. Salomon, J.M. Poutissou and other graduate students for their help and discussions. The operation of TRIUMF by the cyclotron crew is greatly appreciated. I would also like to thank my wife, Yoshiko, for her excellent typing.

I Introduction

A General

The energy-loss of charged particles in matter has been studied, discussed and reviewed in many publications. Tables and figures of range-energy relations which are available in these summaries are useful to experimental physicists in designing and evaluating their experiment. Though the accuracy is somewhat worse than a magnetic spectrometer, the energy of charged particles can be defined quite accurately by measuring their range in matter.

Generally, charged particles lose their energy in passing through matter by excitation and ionization of the atoms and molecules. These processes of energy-loss are similar for all charged particles, but there are some differences between electrons and heavier charged particles (muons, pions, protons, ions, etc). Since an electron is very light, it can lose energy by bremsstrahlung radiation. Although pions, muons and electrons are contained in beam in our experiment, we shall principally discuss the energy-loss of heavy charged particles in this work.

It will be shown later that the stopping power of heavy charged particles depends upon the charge and kinetic energy of the incident particles and to a lesser extent on the material of the stopping medium. If we know the stopping power of one kind of charged particle, then we can apply the scaling relation of the stopping power to any other kind of heavy charged particles. In most articles, the

stopping power and range of protons are discussed.[1-6] Using the scaling relation, we can calculate the stopping powers and ranges of other heavy particles from those of proton.

The experimental results of the range-energy relation for pions produced by the meson facility, TRIUMF, will be discussed in this work. Although the range of protons has been measured for various energy ranges,[1-6] few experimental studies[7] of pion range have been reported. The present experiment concerns the range of pion in aluminum and copper.

The problem of the energy-loss of charged particle passing through matter was discussed in the early part of this century. Bohr[8] considered the problem by classical mechanics, then Bethe[9] treated the problem successfully by using quantum mechanics. A short summary of the theory of stopping power and range in matter will be given in section B.

Reviews of range energy relations have been published every few years. The first extensive summaries were given by Livingstone and Bethe.[10] In 1937, they discussed the theory of straggling and energy-loss of charged particles after traversing a given length of matter. A short summary article was published by Taylor,[11] who summarized the situation up to 1951. Then Allison and Warshaw[12] gathered together all of the stopping power data covering low and high energies in 1953. In 1954, Uehling[13] published a survey on the energy-loss of heavy charged particles. He

reviewed the arguments on which the energy-loss equations are based and also experimental results. The survey of the experimental data covering the energy less than 10 MeV was done by Whaling[14] in 1958. After Uehling's summary, some additional measurements on a proton beam up to 700 MeV have been done. Fano[15] surveyed the literatures including the additional results up to 1963 and reviewed stopping power theory in detail.

Serre[16] calculated the range and the stopping power of various materials (12 kinds) for the wide energy regions from 10 MeV to 30 GeV for protons, kaons, pions and muons. The calculated ranges and stopping powers are in good agreement with experimental values to an accuracy better than 1 % in the energy range from 10 MeV to 1 GeV. In this thesis we mostly refer to her report for numerical values of ranges and stopping powers.

The most recent summary appeared in the American Institute Handbook.[17] In this article are given the most recent references, the commonly used formulae and principal data on the passage of fast charged particles in matter. The tables of stopping powers and ranges are based on calculations using a correction for inner shell electrons and the continuous slowing down approximations. Values are given for proton energies between 1 and 1000 MeV.

The problem of energy-loss in matter is understood precisely as discussed in summaries cited above. But, recently, some miscellaneous effects have been pointed

out in the ranges and Bethe's formula. According to the measurements of Heckman and Lindstrom,[18] the energy-loss rates of positive pions exceed that of negative pions by amounts of 0 to 60 MeV/cm in the velocity interval $0.051 < \beta < 0.178$ ($200 \text{ kev} < E < 2.3 \text{ MeV}$). This is due to the difference in the Coulomb interaction with atomic electrons.

Bethe's formula, which is derived by a quantum-mechanical theory based on the first Born approximation, gives good agreement with the energy-loss experiment of fast particles but does not explain the difference in the range of opposite charged particles. Such an effect is predicted by the second order Born approximation which gives a term proportional to Z^3 of the incident particles. This higher order correction of the stopping power, proportional to Z^3, is discussed by Jackson and McCarthy.[19] They have shown that the Z^3 term at low velocity leads to the range difference for particles of the same mass, the same initial energy, but of opposite charge. Inokuti[20] also indicated the departure from Bethe's formula at low velocity in his summary.

The time of flight method is a relatively simple method for measuring absolute velocity of particles and useful over a wide range of particle types and energies. A review of time interval measurements was given by Porat[21] who discussed the time intervals in the range of pico-second to micro-second. The time of flight method has been reported for measuring cyclotron beam energy,[22-25]

using the cyclotron oscillator as a time standard. The deuteron energy with momentum 1025 MeV/c was measured by the time of flight between two scintillation counters and also by the range measurement.[26] For neutral particles (neutron), the usual techniques applied to charged particles such as a magnetic spectrometer and range-energy relation can not be applied. However, the time of flight method has been applied successfully for measuring the energies of neutrons.[27-29]

Recently the experimental results of measuring the energy of pion by the time of flight have been reported from the meson facilities[30-32] (SIN, LAMPF, TRIUMF). Those machines can accelerate high currents of proton to produce the high intensity of pion beam. From the meson production target, the beam, which includes pions, muons, electrons and other particles produced by the nuclear reaction, is extracted to the experimental area passing through the pion channel. Each particle contained in the beam has the same momentum but the different velocity due to the different mass. Therefore, using the time of flight method, we can identify the particles and determine the velocities in the experimental area.

The present report will show the range measurements of pions in aluminum and copper for the energy region from 30 to 60 MeV. The energies of pions under the same condition are measured by the time of flight method. We shall compare the energy obtained from the range with that of the time of

flight.

In the measurement of the time of flight, we measure the time difference in arrival between electrons and mesons which travel from the pion production target to a detector. As electrons, muons and pions with the same momentum have different energy losses in the plastic scintillator, they have a different triggering time in the leading edge type discriminator. We will discuss the difference in time pick off of discriminators between the leading edge type and the constant fraction in section 3-D.

Since our experiment was done on the M9 channel, where the bending magnets define the particle momentum, we shall be able to utilize the relation between the strength of the magnet currents and the pion energy.

B The Theory of Energy-Loss

The energy-loss of charged particles in matter is quite well understood. It is mainly due to ionization and excitation of the atoms in matter. The nuclear interaction which has a much shorter range than the electromagnetic interaction may become important when the particle has enough energy to come close to the nucleus. We can find the classical calculation of the energy-loss in matter in many elementary books on Nuclear Physics.[33-35]

(1) The Stopping Power of Charged Particles

The classical theory was developed by Bohr.[8] It assumes that an ion with charge Ze and velocity v passes within a distance b from an electron which is assumed to be free and at rest. While the ion is affected by the electromagnetic interaction with the stopping medium, the atomic electrons are assumed to move very slowly. Since the collision time is assumed to be short, they acquire an impulse without changing their position. According to this impulse approximation, the momentum acquired by the electron must be perpendicular to the trajectory of the incident particle and can be calculated by applying Gauss' theorem to a cylinder with the radius b. The momentum gives the classical kinetic energy lost by the ion at an impact parameter b. Then, the rate of energy-loss per unit path length, $-dE/dx$, is given by integrating the classical kinetic energy over b from a minimum to a maximum. Thus, the stopping power of

the absorbing medium was obtained in the classical form.

Bethe[9,10] developed the theory discussed above by considering quantum theory, relativistic effects and shell effects. The Bethe's equation is as follows:

$$-\frac{dE}{dx} = \frac{4\pi z^2 e^4}{m_e v^2} \cdot n Z \left\{ \ln\left(\frac{2m_e v^2}{I}\right) - \ln(1-\beta^2) - \beta^2 - \sum_i \frac{C_i}{Z} \right\} \qquad (1.1)$$

where there are n atoms with atomic number Z in the unit volume of the absorber, and C_i is the shell correction of the i-th shell. Since Bethe's equation is obtained by using the Born approximation for the collision process, it can be applied when the velocity of the incident particle is large compared to the velocity of the atomic electrons.

Bethe's equation depends on the velocity and charge number of incident particles. In order for the equation $dE/dx(m_1,Z)=dE/dx(m_2,Z)$ to hold for two kinds of incident particles of different mass but the same charge, the following relation is needed;

$$\frac{T_1}{m_1} = \frac{T_2}{m_2} = c^2(\gamma - 1) \qquad (1.2)$$

where T_1 and T_2 are the kinetic energy of two kinds of incident particles. From this result, if the stopping power for protons is known, then the stopping power of the particle with mass M_x and one electrical charge is obtained

by shifting the values for proton by a factor M_x/M_p (=0.150 for pion). Similarly, if particles with different Z are considered, the energy-loss of a particle with charge Z_1 is shifted by a factor $(Z_1/Z_2)^2$ from the case of a particle with charge Z_2. For the case of an alpha particle and a proton, $(Z_\alpha/Z_p)^2=4$. In the reference 6, the experimental stopping powers for proton energies of 0.05 to 12 MeV are given. Using the rule to convert the proton stopping power to a pion stopping power, the stopping power for pion energies of 0.05 to 10 MeV is shown in Fig. 1.1 for the case of aluminum and copper.

If the stopping power of a standard absorber at a given energy is known for a certain particle, then, for any absorber under the same energy condition, the stopping power of any absorber can be derived from the ratio

$$Q=\frac{\frac{1}{\rho}\left(\frac{dE}{dx}\right)}{\frac{1}{\rho_s}\left(\frac{dE}{dx}\right)_s}\approx\frac{\frac{Z}{A}\ln\left(\frac{2m_eV^2}{I}\right)}{\frac{Z_s}{A_s}\ln\left(\frac{2m_eV^2}{I_s}\right)}=\text{Const.} \qquad (1.3)$$

This is called the relative stopping power and is used to calculate the thickness of different materials relative to the standard absorber. In this report, this relation will be used to calculate the relative thickness of plastic scintillator to aluminum and copper absorbers.

(2) Range of a Charged Particle

Since the equation for the energy-loss of charged

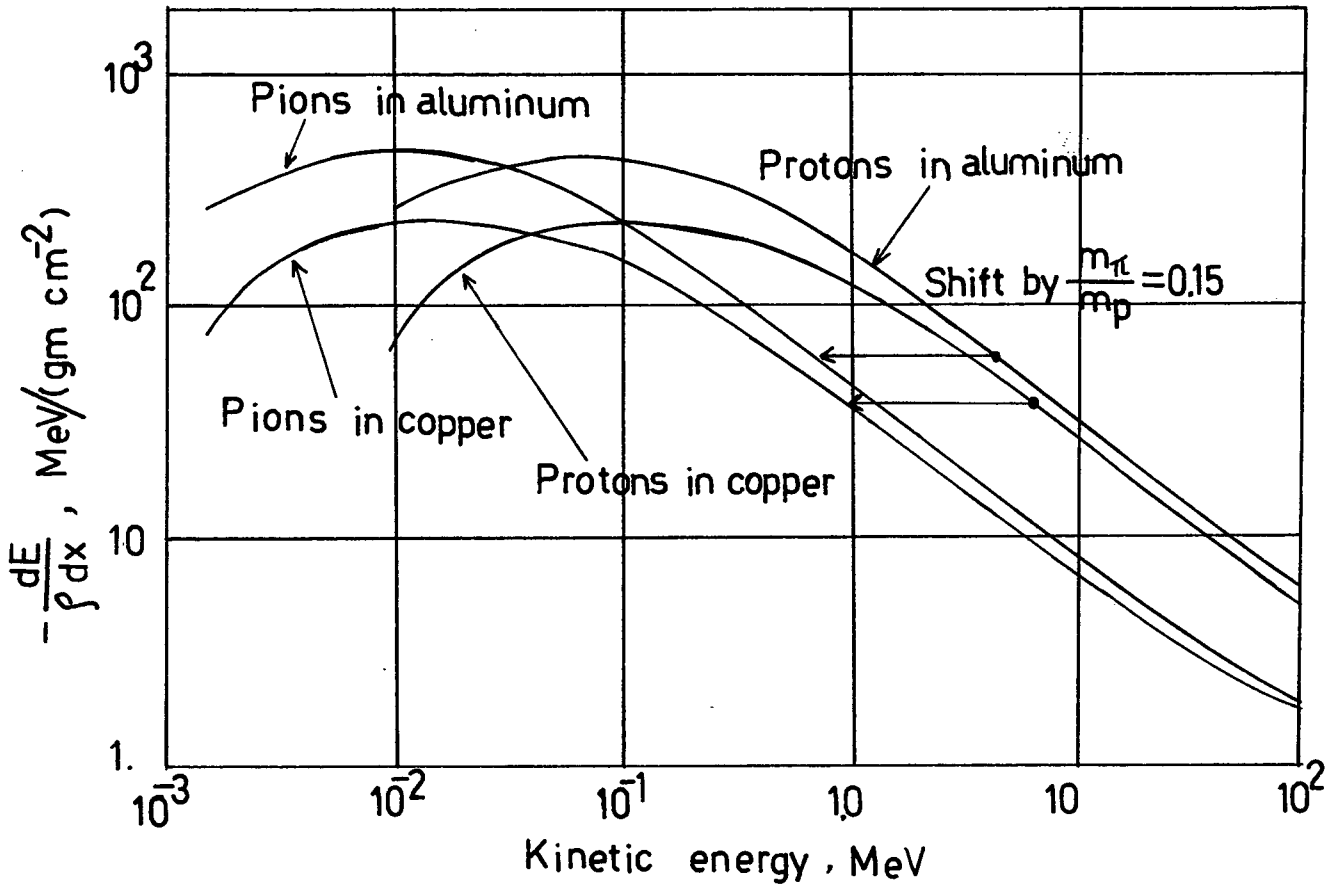

Fig. 1.1 Energy-Loss curves for different charged particles in aluminum and copper.

particles is obtained in the last section (1), it is possible to integrate from the initial incident energy to the energy at rest to find the total range of traversing particles in matter. We have

$$R(E_o) = \int_0^{E_o} \frac{dE}{-\left(\frac{dE}{d\chi}\right)} \tag{1.4}$$

where the continuous slowing-down approximation is applied to the integration. Since the stopping power depends on the particle velocity and charge, we can obtain the range of particles from the known range for a certain particle by a scaling rule. It is difficult to use the equation of stopping power to get the range at low energy, since the theory has been obtained by using the approximation that the incident particles have high enough energies to assume that the atomic electrons are at rest, as discussed in the last section. This gives a little uncertainty to the integrated range. In order to avoid this uncertainty, the integral can be separated into two energy regions, i.e., $0 < E < E_1$=1 MeV and $E_1 < E < E_0$. Then, for the low energy region, the experimental data shown in Fig. 1.1 can be used.[17] For the high energy region, the stopping power equation can be used successfully. In the reference 16 to which we will mostly refer in this work, the experimental results of Barkas[36] have been employed for the low energy region.

II Experimental Equipment

A Pion Production

The extracted proton beam from the TRIUMF cyclotron can be varied in energy continuously from 150 to 520 MeV. In this experiment, the 500 MeV proton beam was provided by the cyclotron and the current was kept in the range of 1 to 5 nano-amps. The cyclotron radio frequency is 23.04 MHz which corresponds to a 43.403 nsec-period. When the R.F. signal was fed to the Time to Amplitude Converter (TAC, ORTEC 437A) as the stop signal for the time of flight measurement, every second pulse of the R.F. signal was erased to produce two peaks in the time spectra for a single type of particle.

In this experiment, the beryllium target of 10 cm thickness was used mainly for the meson production target because of the high production rate. Since, for a target of low atomic number, the production rate of electrons is small, the copper production target was employed to compare the peak position of electrons in a time-delay spectrum with the case of beryllium target. The result and discussion will be given in the section 3-D. Also a CH_2 target was used to measure the effect of the thickness of a stopping plate between the third and fourth counter (Fig. 2.4).

The pions, muons and electrons produced at the T2 target pass through the M9 channel which is at 135° to the direction of the proton beam (Fig. 2.1).

We can choose positive or negative pions by changing

the polarity of the magnets. Since the positive pion production is larger than the negative pion production,[37] positive pions were employed in our experiment. Furthermore, negative pions are captured by nuclei at the end of their range and the reaction produces particles and photons. As these particles produce a background signal, the range curve for a positive pion is generally cleaner than that for a negative pion.

B M9 Pion Channel

The layout of M9 channel is shown in Fig. 2.1. The fixed part of the M9 channel consists of five quadrupole magnets, two bending magnets and the collimating slit. The slit is set between the first bending magnet and the third quadrupole magnet so that we can adjust the beam size. It has 30 cm x 30 cm beam size when wide open and in our experiment we used 2 cm width of horizontal slit and 10 cm width of vertical slit. After the fifth quadrupole magnet, the meson beam enter the experimental area through a vacuum window. In the experimental area, there are two places for setting counters. The first position right after the fifth quadrupole magnet is called F-2, (the second focus). The second position is behind the Corvallis magnet and called F-3, (the third focus). When F-3 is used, the triplet quadrupole magnet is installed in the place of F-2 to focus the beam down to F-3. In this experiment, both positions were used because of the experimental schedule of other groups. From the point of view of the separation of particles in the time-delay spectrum, F-3, which has long distance from the target, is better than F-2. But the flux at F-2 is larger than that at F-3.

The pion energy is defined by the two bending magnets and the profile of beam is shaped by the eight quadrupole magnets. The effects on beam energy of varying the current for the each magnet have been calculated.[38] Therefore, in order to define the momentum of the pions, we can set the

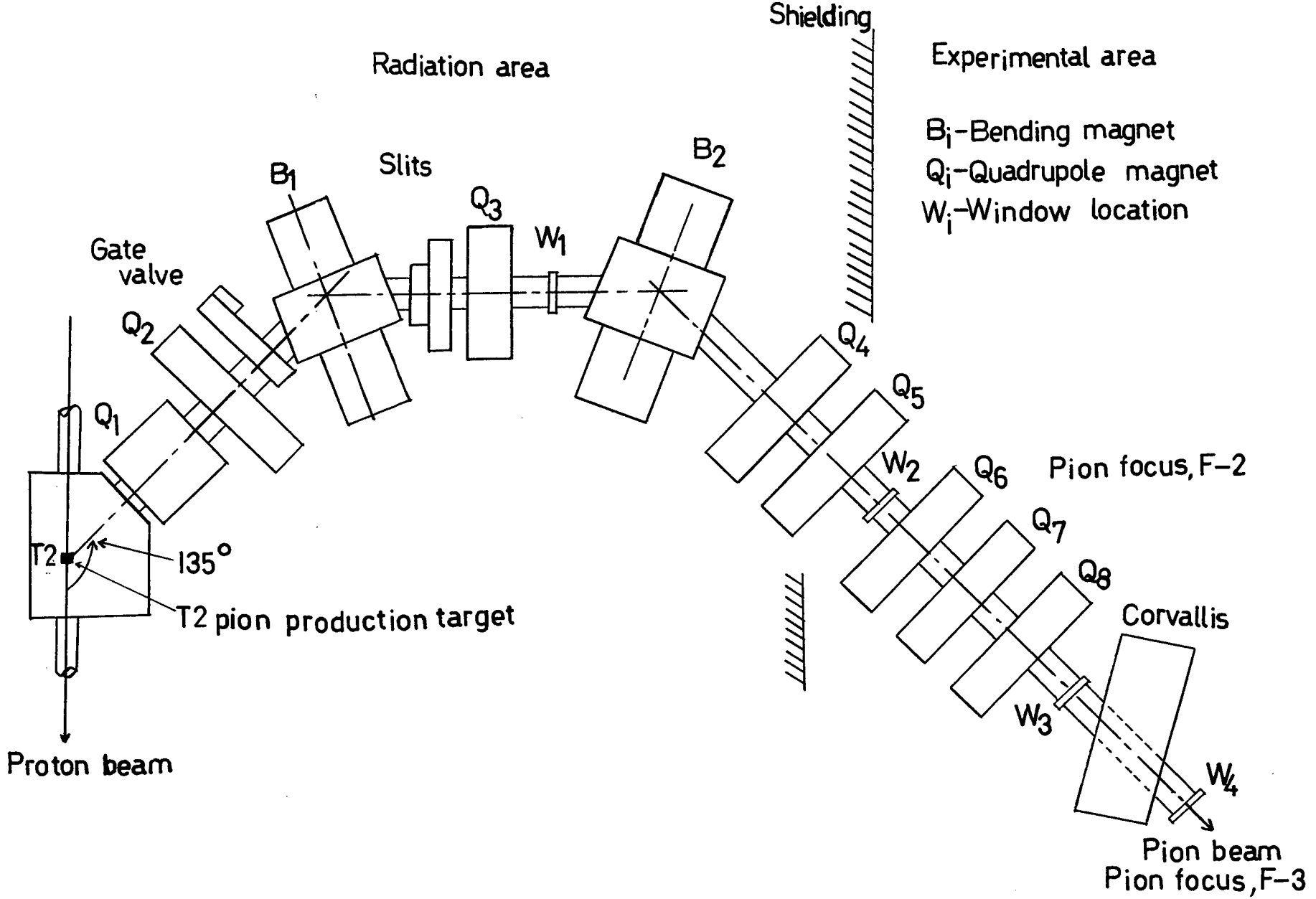

Fig. 2.1 M9 pion beam channel

current of each magnet according to the table 4.1. Then, in order to get the optimum beam of mesons, we can adjust the currents of the second bending magnet and the eight quadrupole magnets while holding fixed the current of the first bending magnet.

The energy defined by the magnets was checked by using the pion produced from the reaction, $p+p \rightarrow \pi^{+}+d$.[39] The pion kinetic energy as a function of angle is shown in Fig. 2.2 for the proton energy from 300 to 600 MeV.[40] The initial pion energy of the M9 channel has to be obtained by considering the thickness of the CH_2 target as shown in Fig. 2.3. To calculate the mean energy of the beam we assume that the pions are produced at the middle of the CH_2 target. The energy-loss of 500 MeV protons in the CH_2 target (1 x 1 x 0.5 cm) is 2.9 MeV and at the middle of the target it has lost a half of 2.9 MeV. As the energy-loss is not so large and within the uncertainty of beam energy, it is assumed that the pion is produced by the reaction of 500 MeV proton at the center of the target. Thus, the pions produced have an energy 30.9 MeV[41] at 135° as shown in Fig. 2.2. Then the pion energy is reduced by the amount of 1.5 MeV in the CH_2 target. Therefore the pions produced at the middle of target have an energy 29.4 MeV at the surface of target. Thus when we adjust the magnets to obtain a nominal 30 MeV pion beam produced by the $pp \rightarrow \pi^{+}d$ reaction, the magnet currents actually correspond to a pion energy of 29.4 MeV.

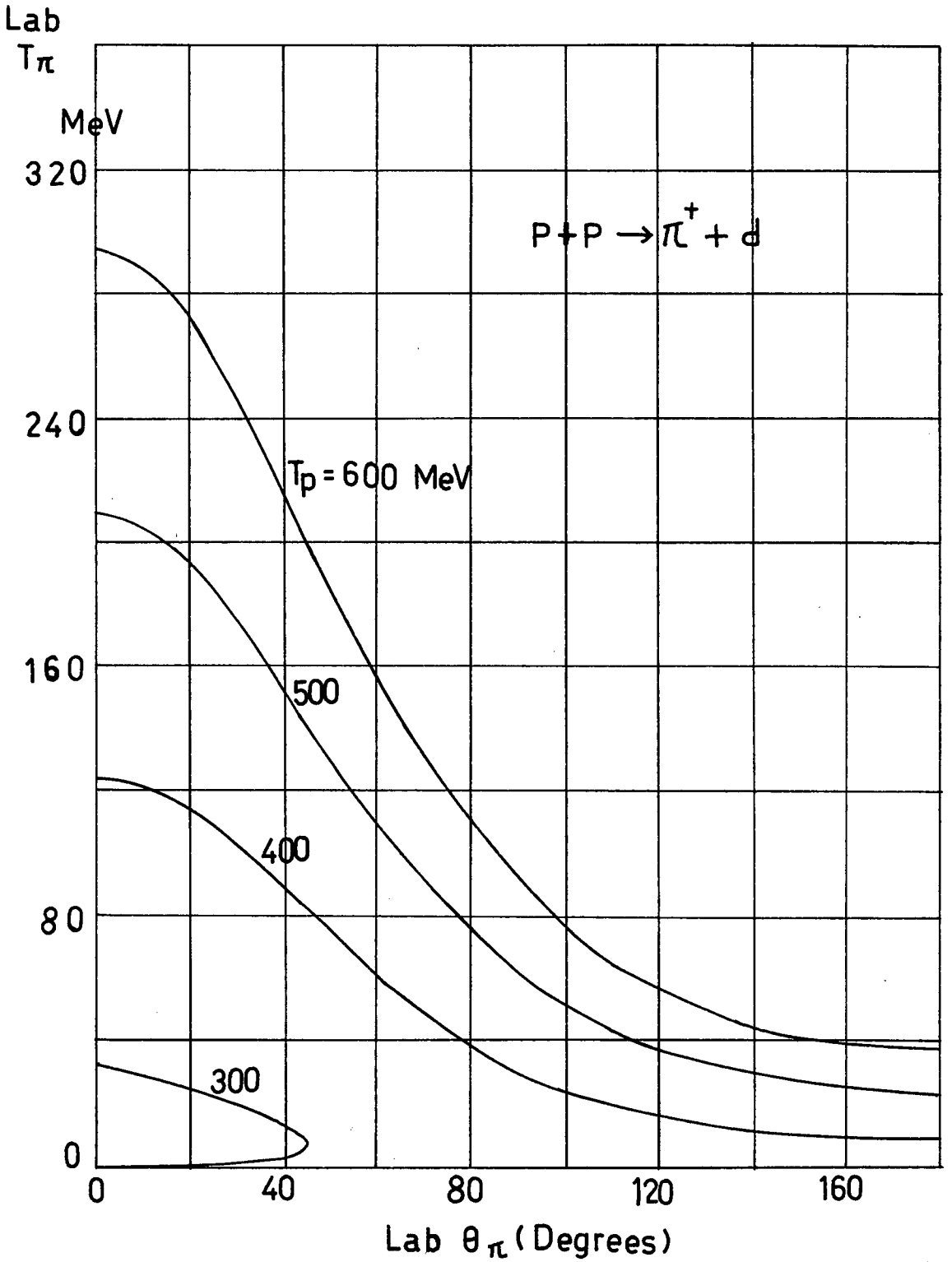

Fig. 2.2 Pion kinetic energy vs. angle in a laboratory system.

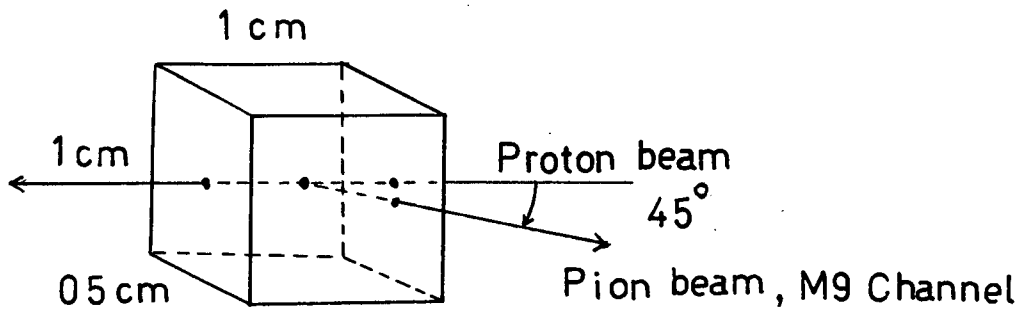

Fig. 2.3 CH_2 target

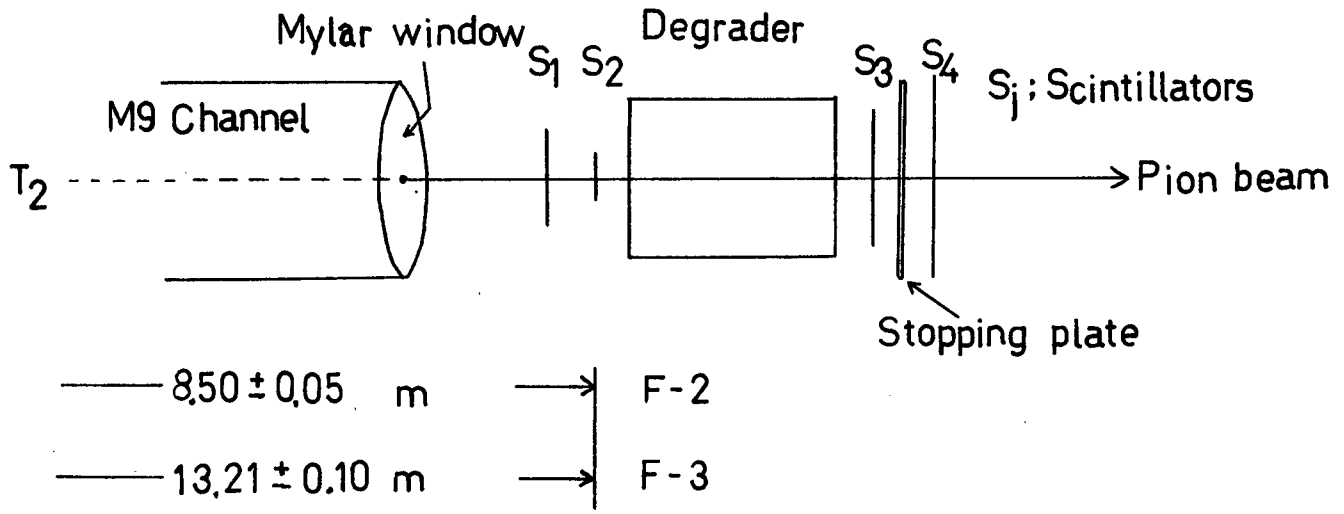

Fig. 2.4 Configuration of counters and degrader

C Counters and the Degrader

After emerging from the vacuum pipe of the M9 channel, which has the seven magnets inside of the radiation area, the mesons come out into the experimental area called F-2. The vacuum is enclosed by mylar window with 0.025 mm thickness. As explained in the section B, there is another experimental area F-3 after the triplet quadrupole and Corvallis magnet. In the experimental area, four scintillation counters with a plastic scintillators (NE102A)[42] were set to measure the range and time of flight. NE102A has the fast decay time of 2.4 nsec and the ratio H:C atoms of 1.104. A RCA 8575 photomultiplier was used and has an anode pulse rise time of 2.5 ns. The layout of the four counters is shown in Fig. 2.4 and the cross-section and the thickness of plastic scintillators are shown in table 2.1. Each plastic was wrapped in black vinyl tape to exclude light. The thickness of the black vinyl tape, 180 microns, must also be considered when calculating the pion range. A small size of the plastic scintillator (5 cm x 5 cm) was used especially for the second counter to define the small beam profile in front of the degrader. Since the beam spreads out after passing through the absorber, the plastic scintillators of the third and fourth counter were made quite large. The fourth counter which gave anti-coincidence signal had a cross-section of 20 cm x 20 cm. The cross-section of the first counter (10 cm x 10 cm) was larger than that of the second counter (5 cm x 5 cm). The

NO	THICKNESS	SIZE	MATERIAL	PHOTO MUL
S_1	0.64 cm	10x10 cm^2	PLASTIC; NE 102A DENSITY; 1.03 g/cm^3 H/C; 1.104	RCA 8575
S_2	0.16	5x5		
S_3	0.16	15x15		
S_4	0.32	20x20		

Table 2.1 The specification of plastic scintillators and photo-multiplier used for counters.

coincidence signal of the first and second counter was used to define the number of incoming pions. The area of the first counter is larger than that of the second counter so that the beam is defined almost entirely by the second counter only.

The degrader, which was set between the second and third counter, has six plates of absorber which can be moved independently by air pistons. It can vary the total range from 0 to 21.3 g/cm^2 for copper and from 0 to 13.9 g/cm^2 for aluminum. Each plate of absorber has a cross-section 18 cm x 18 cm square. The thicknesses of the plate used for the degrader are shown in table 2.2. These thicknesses were measured by a micrometer which was accurate to 2.5 micron. The plates were measured a cm or so in at the four corners and the average of these numbers was taken. It was found that all plates had a constant thickness within 0.2 % deviation (table 2.2). The plates were made of commercially available alloys and the composition is shown in table 2.2. All aluminum plates and thin copper plates had a well-finished surface and were polished with fine sand paper to clean the surface before the experiment. The thick copper plates with 1.1 cm thickness were ground by a local machine shop so that the thickness was uniform to within 30 micron.

PLATE NO	COPPER	ALUMINUM
	COPPER 99.5 % LEAD ZINC IRON 0.5 % DENSITY 8.93 g/cm^3	MAGNESIUM 1.0 % SILICON 0.6 % CHROMIUM 0.25 % COPPER 0.25 % ALUMINUM 97.9 % DENSITY 2.70 g/cm^3
1	0.273 ± 0.0012 g/cm^3	0.218 ± 0.0005 g/cm^3
2	0.728 ± 0.0013	0.443 ± 0.001
3	1.388 ± 0.0027	0.897 ± 0.001
4	2.890 ± 0.0034	1.770 ± 0.001
5	5.787 ± 0.005	3.537 ± 0.002
6	10.241 ± 0.011	6.992 ± 0.007
TOTAL	21.307 ± 0.013	13.857 ± 0.008

Table 2.2 Components and thicknesses of absorbers used for the degrader.

D Electronics

The schematic diagram of the electronics for the range measurements is shown in Fig. 2.5. In this experiment, both the differential range curve and integral curve were taken. In order to take the differential curve, the counts of coincidence in the first, second and third counter with the anti-coincidence of the fourth counter were normalized by the counts of coincidence in the first and second counter. The coincidence of the first and second counter gives the number of particles which pass through both counters. Most of these particles are expected to have emerged from the M9 channel. These particles are electrons, pions and muons. Each signal from four detectors is fed to each discriminator. The output from the first, third and fourth counter are fed to the leading edge type discriminator (LRS quad-discriminator). The constant fraction discriminator (ORTEC 463) is used only for output from the second counter. The difference between the leading edge type and constant fraction discriminator will be discussed in the following chapter. The output from the LRS quad-discriminator is a rectangular pulse of which the width is variable with the amplitude of 0.8 volt. The width of output from the first and third discriminator is 20 nsec wide and from the fourth discriminator 200 nsec wide. The output of constant fraction has a width less than 10 nsec. The wide rectangular pulse is used for the fourth output which is the anti-coincidence signal in order to overlap completely the signal from another discriminator.

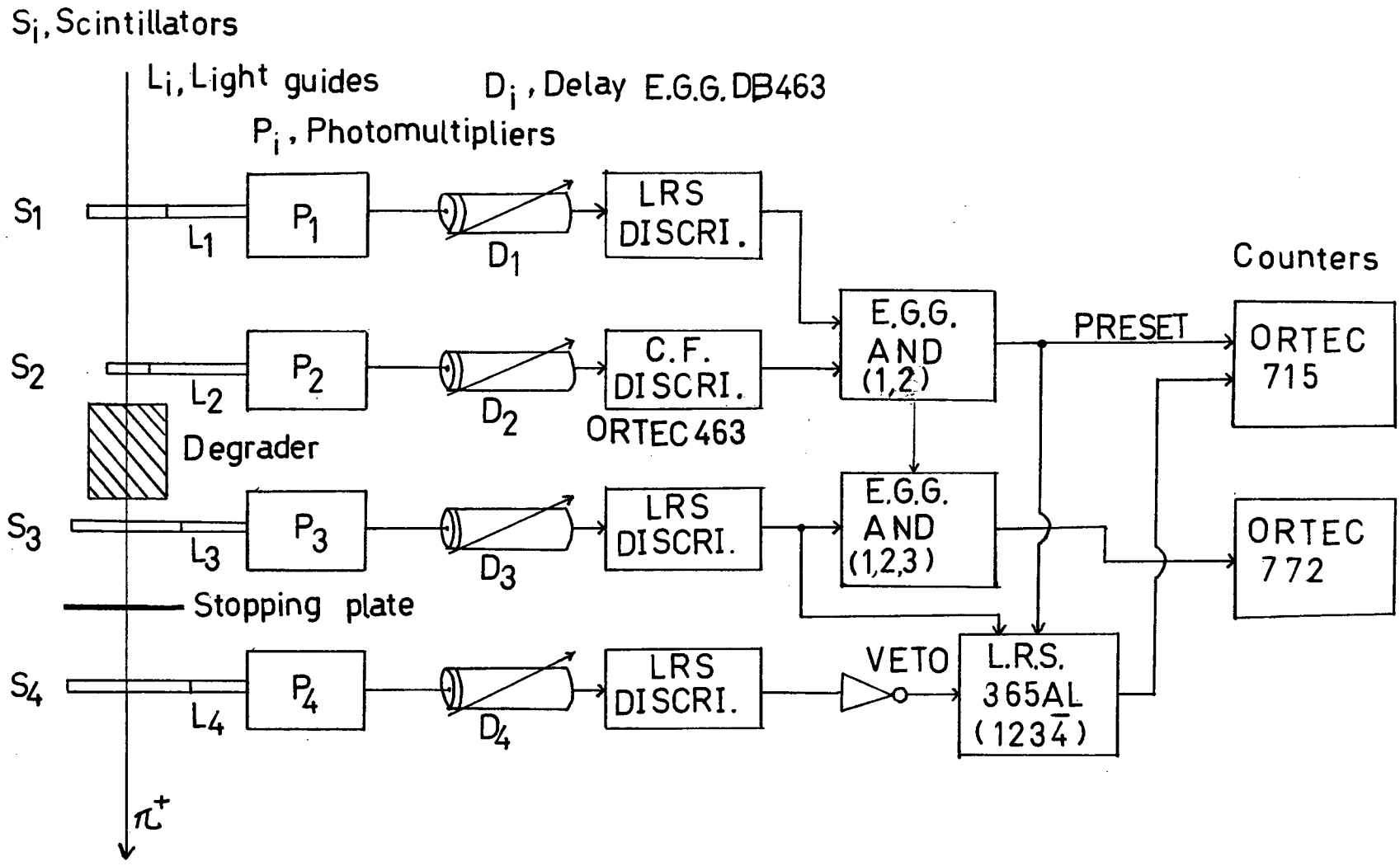

Fig. 2.5 Scheme for the measurements of the range curve

The signal for the time of flight is the output of the coincidence between the first and second counter. It is important to define the distance from the pion production target to measure the time of flight. Therefore, if the coincidence signal is fed to the time-to-amplitude converter (TAC, ORTEC 437A) we have to know which signal of two counters is a start or stop signal. In order to make sure that the second discriminator signal always triggers the coincidence signal, the second discriminator is adjusted to give the narrow pulse. Furthermore, it is important to use the constant fraction discriminator to feed the start or stop pulse to the time-to-amplitude converter instead of the leading edge type discriminator. The effects of these discriminators in the time of flight will be discussed in the following chapter. The R.F. signal is employed as a stop signal, because the frequency of the R.F. is too high to use the signal as a start signal for the TAC.

The output of the TAC is analyzed by the multi-channel analyzer (Northern Scientific Model, NS 900) and the time delay spectrum of the analyzer is typed out by a teleprinter. The count of the (1,2) coincidence is used as the preset count in the dual counter/timer (ORTEC 715) and $(1,2,3,\bar{4})$ coincidence is counted. This will be discussed in detail in the following chapter. When the count rate is high, 10^4 of preset count is employed but, when it is low, a half of 10^4 is employed.

III The Basic Experiment for the Measurement of the Range-Energy Relation and Time of Flight

There are several methods to measure the momentum and energy of charged particles. In our experiment, the energy of pion was defined by three methods, the range-energy relation, the time of flight and the bending magnet current. In this chapter, the basic idea and fundamental problem in measuring the range and the time of flight will be discussed.

A The Range Curve

When charged particles pass through matter, they lose energy by ionization. If we know the range in matter, the energy of charged particles can be obtained. In our experiment, the energy of a positive pion is determined by its range in aluminum and copper. In the section 2-D above, the method of measurement of range has been shown briefly. The coincidences $(1,2,3,\bar{4})$ and $(1,2,3)$ give the differential curve and integral curve, respectively. The number enclosed with parentheses signifies the counter in Fig. 2.5 and the bar on the head of the number 4 designates that it is an anti-coincidence signal from the fourth counter. The example of the differential and integral range curve is shown in Fig. 3.1. These data were taken using a CH_2 pion production target under the condition that the pions were stopped in a 0.16 g/cm^2 thick scintillator, the horizontal slit was closed to 2 cm and the absorber used was aluminum.

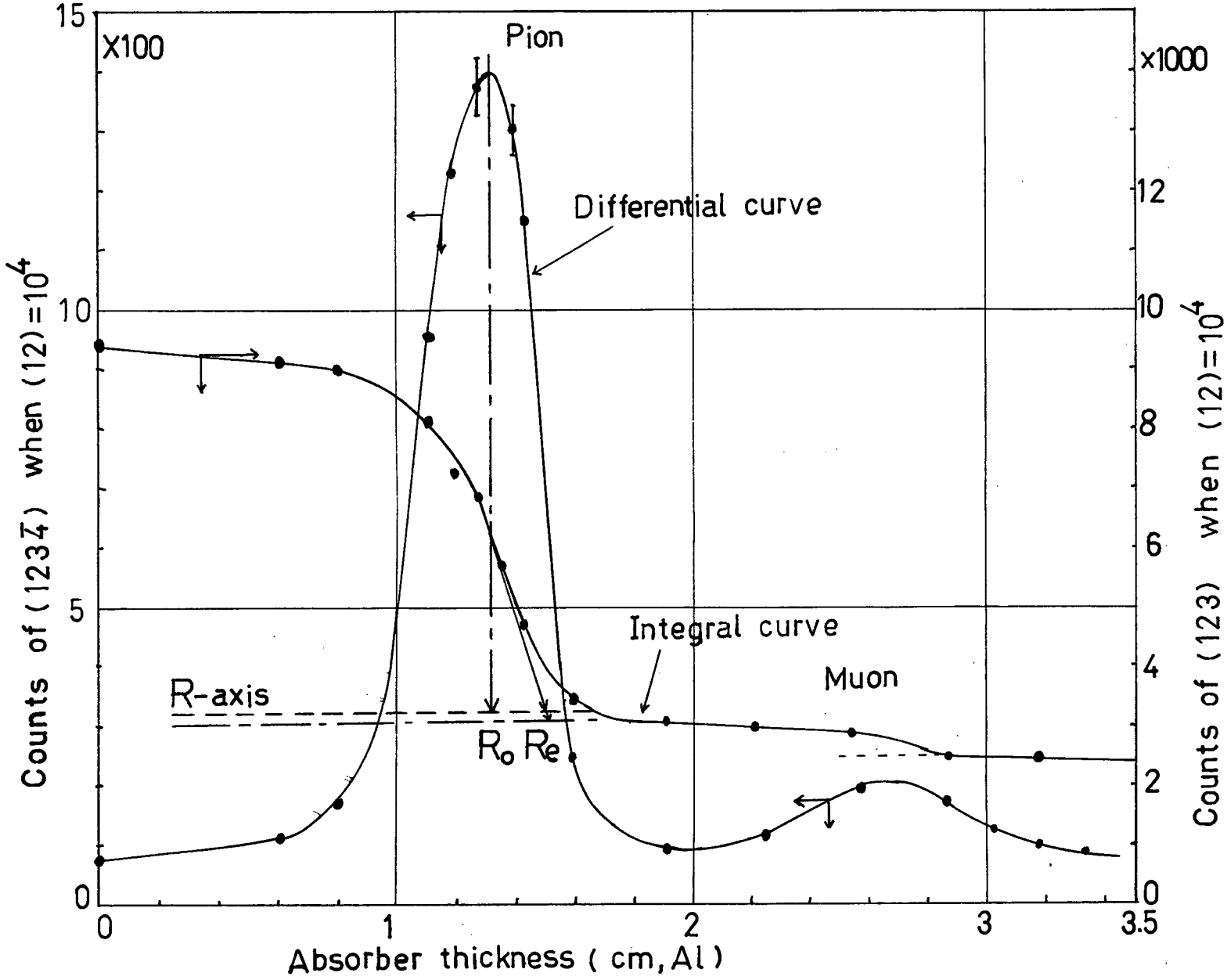

Fig. 3.1 The differential and integral range curve for 30 MeV pion stopped by Al.

With no absorber and perfect geometry, one might expect that the counts of $(1,2,3,\bar{4})$ and $(1,2,3)$ would equal 0 and 10^4, respectively, for the case of $(1,2)=10^4$. But as shown in Fig. 3.1, $(1,2,3,\bar{4})=80$ and $(1,2,3)=9400$ without the absorber. This means that 600 particles out of 10^4, which fire the first and second counter, go aside to miss the third counter. As the absorber thickness increases, the differential curve shows clearly two peaks. One of them is the pion peak and the other the muon peak. These peaks result from the stopping of pions and muons in the scintillator of the third counter. So, as the matter which stops the particles increases, these peaks get much higher. The pion peak is higher than the muon peak due to the higher percentage of pions in the beam. The pions and muons have different ranges because the two particles have the same momentum but different energies (the muon mass is 105.7 MeV/c^2 and the pion mass is 139.6 MeV/c^2). We also observe an electron peak but the peak position is off scale due to the large range.

The distribution of two peaks should be Gaussian. When a beam of particles loses energy by ionization, the particles do not all stop after passing through the same thickness of material. The probability of a particle stopping within dR of R, P(R)dR of a particle, is given by

$$P(R)\,dR = \frac{1}{\alpha\sqrt{2\pi}} \exp\left\{-\frac{(R-R_0)^2}{2\alpha^2}\right\} dR \qquad (3.1)$$

where R_0 is the mean range obtained by integration over the average energy-loss (Eq. 1.4) or, equivalently, from the position of peak on the differential range curve.

In Fig. 3.1, the integral range curve shows two slopes around the peaks of the differential curve. The first and second slope give the range of pion and muon, respectively. The mean range of the particles can be obtained from the integral curve. In the figure, we find that the pion step has its half value at $R=R_0$, which is the position of the peak of the differential curve. By drawing a tangent at the steepest point of the pion slope and obtaining the intersection of the tangent with the R-axis, we find the extrapolated range,[10,43] R_{extr}, which is given by

$$R_{extr} = R_o + \sqrt{\frac{\pi}{2}} \cdot \alpha \qquad (3.2)$$

The difference $R_{extr}-R_0$ is defined as the straggling parameter S.

Since it is clear from Fig. 3.1 that both the integral and differential curve give the same range, we will use the differential curve to define the range of particle in matter by using Gaussian curve fitting.

B The Height of Peak in the Differential Range Curve

In the last section it was noted that the particles which are counted in the differential range ($1,2,3,\bar{4}$) must be counted in scintillator #3 yet not be counted in scintillator #4. These pions must therefore stop some way into scintillator #4 (or in the wrapping material). In our experiment a thin plastic scintillator (0.16 g/cm^2) was used for the third counter to reduce the absorption of the pion. It was expected that the width of peak in the range curve might be narrower by using the thin scintillator for the third counter without any absorber between the third and fourth counter. The width of the peak is caused mostly by the initial energy spread of beam and the stragglings in the degrader and plastic scintillators contribute a little to the width. If there is an absorber behind the third counter, the energy straggling is increased and the width of peak seems to be wider. In order to see the effect of the thickness such an absorber behind the third counter, the range curves were taken for three cases; (1) no absorber, (2) with 0.8 mm thickness aluminum absorber, (3) with 1.5 mm thickness aluminum absorber. For this test, 30 MeV pions were employed and the CH_2 target was used at the T2-target.

The range curves are shown in Fig. 3.2. This experiment was performed on the F-3 position behind the Corvallis magnet. The experimental arrangement is shown in Fig. 2.4 and the currents of bending magnets and quadrupole magnets

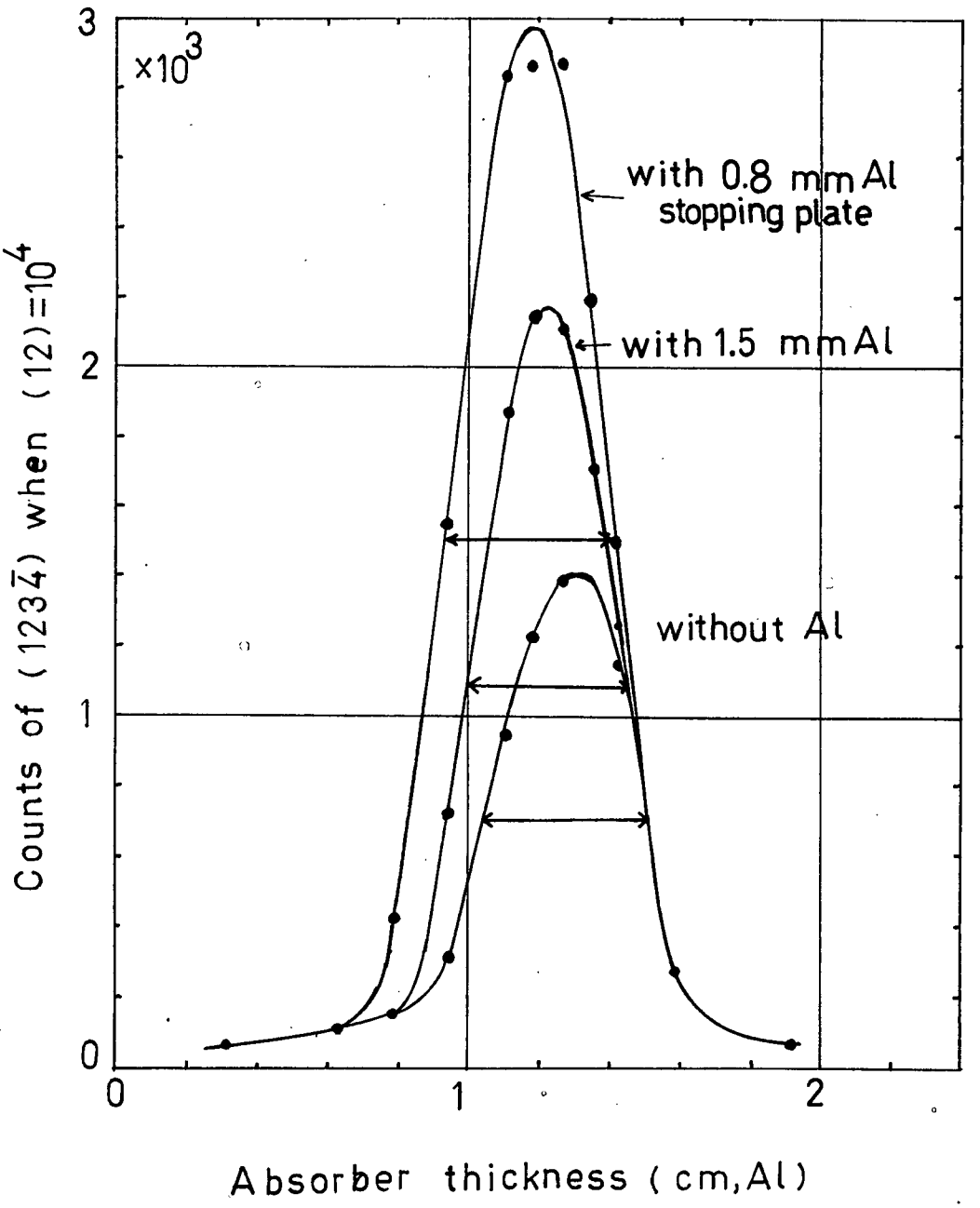

Fig. 3.2 The effect of the stopping plate between the third and fourth counter.

are given in table 3.1. The results are shown in table 3.2. Fig. 3.2 shows that the peak with Al absorber is higher than the case without the absorber and peak positions shift according to the thickness of the absorber behind the third counter. The total ranges of the three cases (correcting for the additional absorber) are given in table 3.2 and agree very well each other. Also the energy obtained from the range is consistant with the energy from the measurement of the time of flight. Therefore, from the energy point of view, it does not matter whether the absorber behind the third counter is added or not. But from the point of view of measurement, as seen from Fig. 3.1, the stopping rate with the absorber is greater than the stopping rate without the absorber. It is also clear from the table 3.2 that there is not a great change in the full-width half-maximum even with the aluminum absorber. As the measurements for this thesis were made with a small proton current (between 1 and 5 nA), a stopping plate was used in our range experiment to improve the count rate; as a compromise the thickness chosen was 0.8 mm of aluminum plate.

MAGNET	CURRENT* (Amp.)	MAGNET	CURRENT* (Amp.)
B_1	245.5	Q_4	168.9
B_2	247.0	Q_5	178.6
Q_1	168.1	Q_6	205.3
Q_2	163.7	Q_7	167.4
Q_3	128.7	Q_8	119.0

Table 3.1 The currents of magnets for the measurement on F-3.

* The numbers in the table actually show the voltage which is an output of the amplifier, 0-50 mV→0-5 V. It amplifies the voltage across the shunt, 50 mV-500 A, $\pm$0.25%, which is installed in series with the magnet. Thus the reading of the amplifier gives directly the amount of magnetic current.

THICKNESS OF ABSORBER	000 mm	0.8 mm	1.5 mm
PEAK POSITION (g/cm^2)	3.59±0.24	3.38±0.22	3.29±0.23
RANGE OF ALUMINUM INCLUDING THE THICKNESS OF STOPPING PLATE (g/cm^2)	3.62±0.24	3.51±0.22	3.51±0.23
HALF WIDTH OF PEAK (g/cm^2)	1.30	1.20	1.32
CORRECTION FROM PLASTIC AND VINYL COVER IN ALUMINUM RANGE (g/cm^2)	1.19	1.29	1.29
TOTAL RANGE IN ALUMINUM RANGE (g/cm^2)	4.81±0.25	4.80±0.23	4.80±0.24
ENERGY OBTAINED FROM ALUMINUM RANGE (MeV)	29.3±0.9	29.3±0.8	29.3±0.8
ENERGY OBTAINED FROM THE TIME OF FLIGHT METHOD (MeV)	30.02±0.87		

Table 3.2 The effect of the stopping plate to the pion energy determination and the comparison of energy between the range and time of flight method.

C The Principle of the Time-of-Flight Method

The M9 meson beam channel is shown in Fig. 2.1. The 500 MeV proton strikes the T2 target and produce pions (as well as heavier ions such as deuterons, alphas, etc.). Some of the charged pions decay into muons; the neutral pions all decay into two gamma rays which immediately create electron-positrons pairs in the surrounding material. All these particles, emitted at 135°, form into the M9 beam. As all these events occur very quickly, the time structure of the M9 beam is always related to the time structure of the proton beam and thus to the R.F. of the accelerator. In our experiment, signals of the R.F. and the scintillation counter were employed to measure the velocity of particles.

The electronics for the time of flight is shown in Fig. 3.3. We used the time-to-amplitude converter (TAC, ORTEC 437A) and multi-channel analyzer (N.S. 900) to measure the time of flight of particles from the T2 production target to the scintillation counter in the experimental area. In this type of time-interval measurement, the output voltage of the TAC is linearly proportional to the time difference $t_2 - t_1 = \Delta t$, where the arrival of the start pulse and the stop pulse is at t_1 and t_2, respectively. The timing diagram (Fig. 3.4) shows the start and stop, the time difference counted by the TAC and the place of each particle on the MCA. Since the high frequency signal of the R.F. can not be accepted as the start pulse, the R.F. signal is fed to

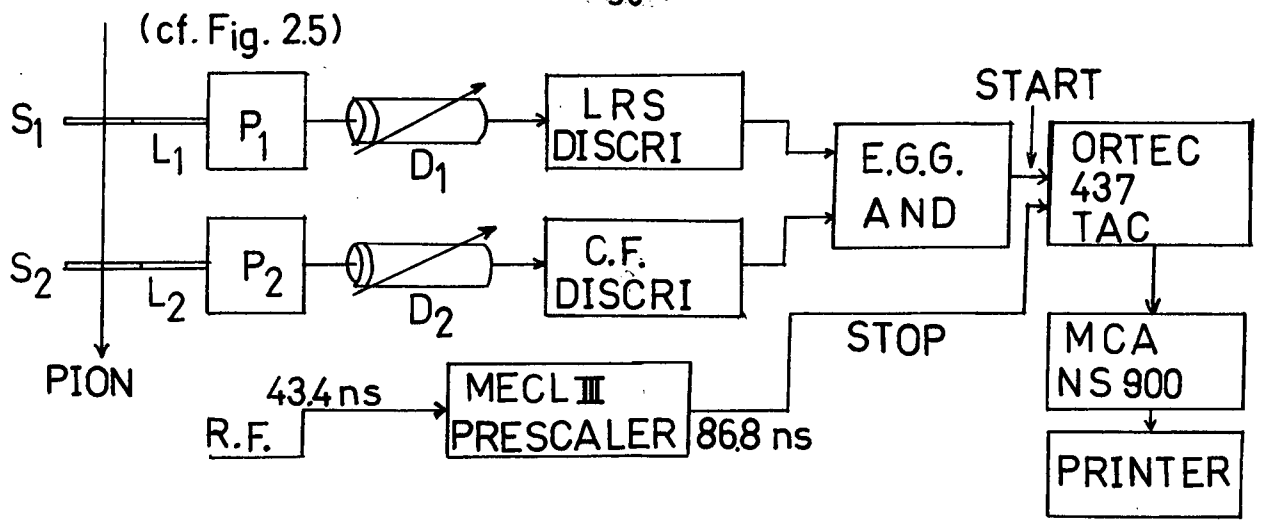

Fig. 3.3 Circuit diagram of the time of flight measurement.

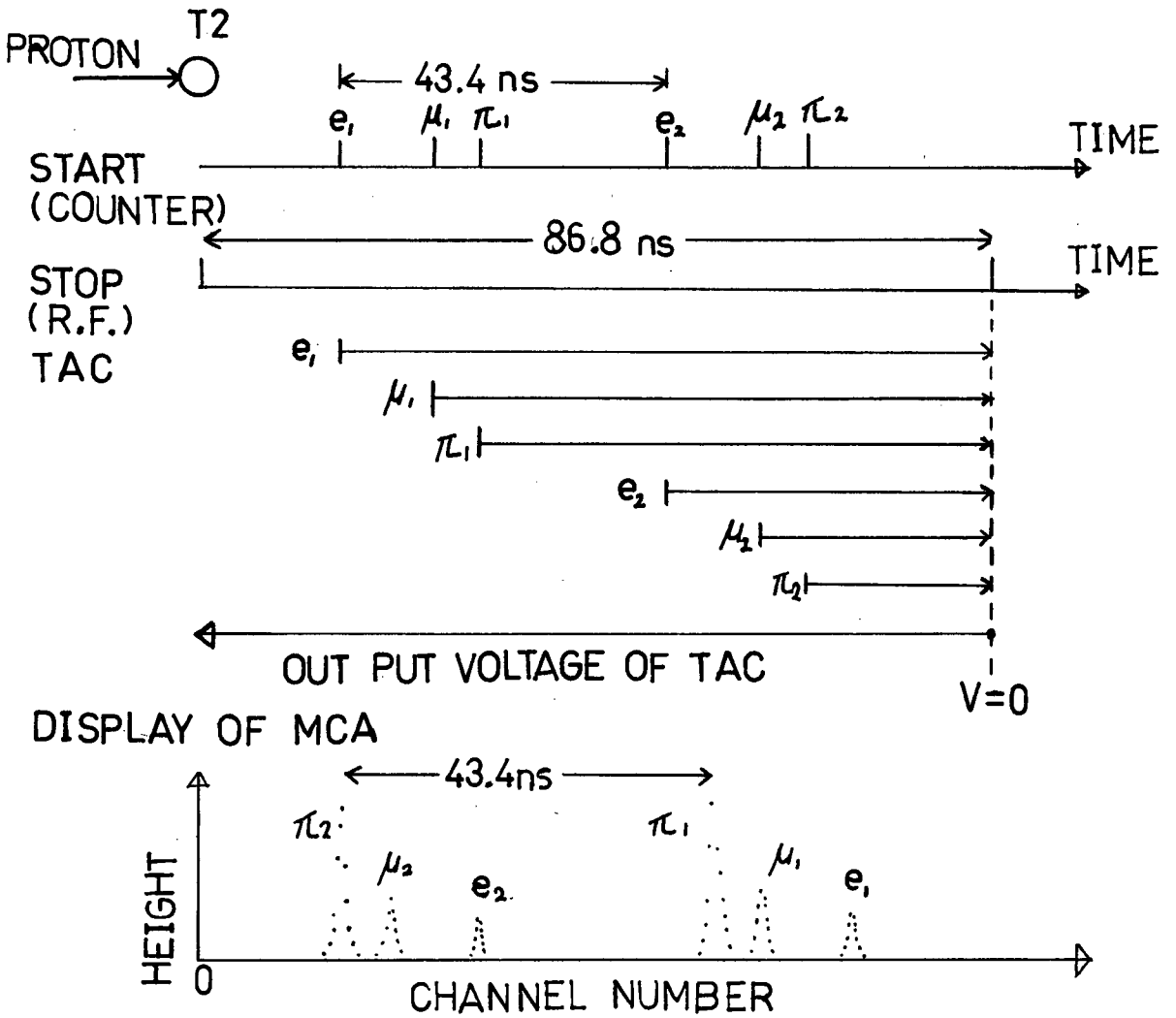

Fig. 3.4 Timing diagram of TAC and the display of particles on the multi-channel analyzer.

the stop and the signal of the scintillation counter to the start as shown in Fig. 3.4. Consequently, the order of particles on the MCA is reversed so that the electron peak appears after the pion and muon peaks.

The R.F. has a 43.4 nsec repetition time but in our experiment a scale of two was added to the R.F. pulses, thus providing a stop pulse every 86.8 nsec. Therefore, there are two peaks for each particle in the time-delay spectrum. Since these two peaks have a time difference of 43.4 ns, this gives natural calibration for the MCA. We also calibrated the MCA using the time calibrator (ORTEC 462). The calibration results are shown in Fig. 3.5. The periodic input of 10 ns signal is fed to TAC. (The time calibrator produces a pair of pulses separated by 10, 20, 40 and 80 ns; the specifications of the instrument indicate that the error is $\pm$10 psec for the 10 nsec interval and 0.005 % for the other intervals.) As shown in Fig. 3.5, all peaks are almost equally separated and each channel corresponds to 178 psec. Since the MCA shows good linearity, the uncertainty of the MCA is negligible in our experiment.

In order to calculate the velocity of particles, we have to know the distance from the T2 to the counter which gives the start signal to the TAC and, also, the time difference in arrival at the counter between the electron and another particle. Assuming that the electrons travel with the velocity of light, the time of flight for electron from T2 to the counter is known. Then, adding the time difference between

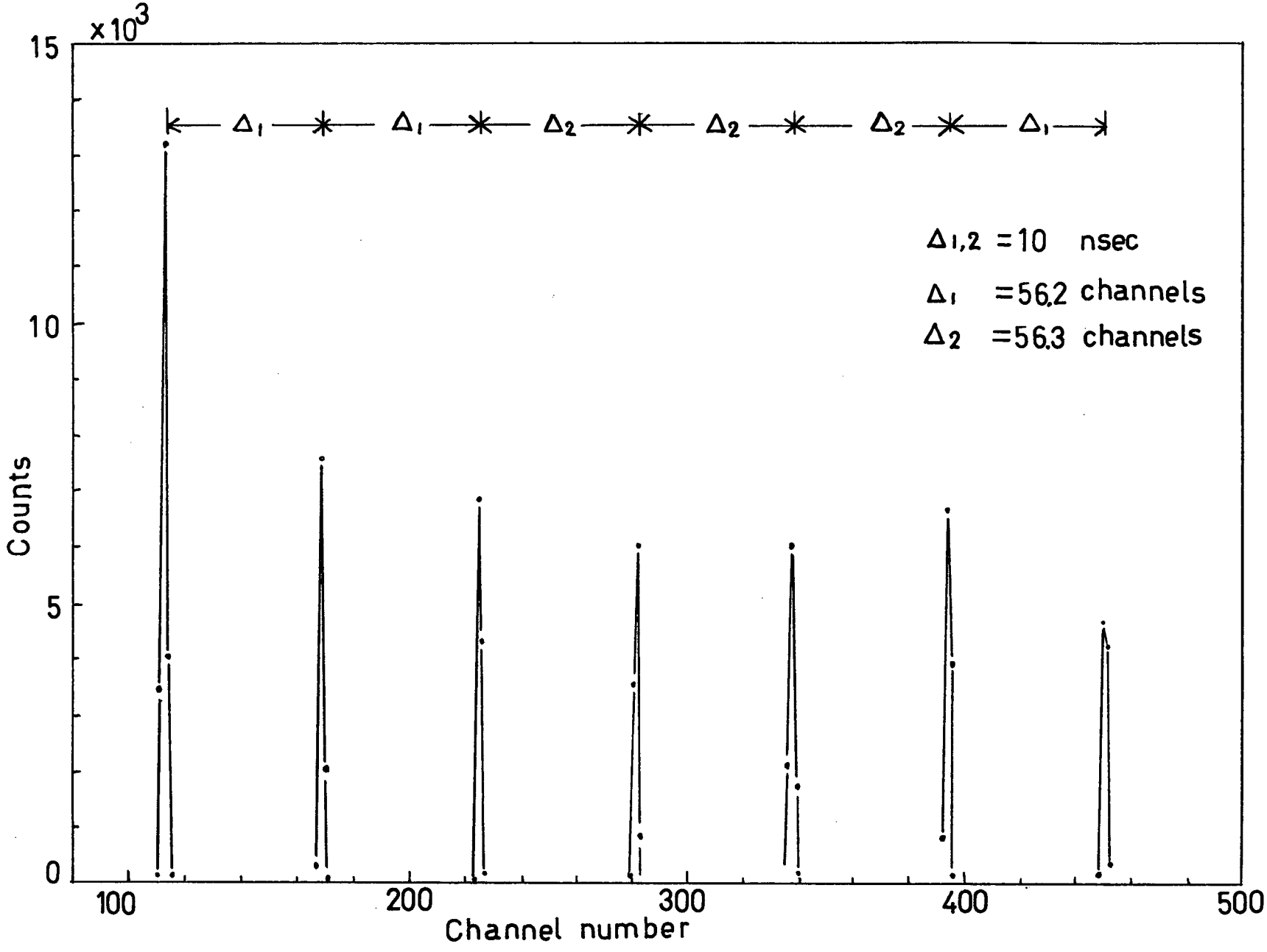

Fig. 3.5 Time calibration spectrum (periodic input, 10 nsec)

the particle and electron, the time of flight for the particle is calculated. This time gives the velocity of the particle.

D The Time Walk of the Discriminator[44]

In the time of flight measurement, the problem of time walk arises from the discriminator. Since this gives serious difference in the particle energy, we have to choose the suitable discriminator. The time walk of discriminator is caused by the different energy-loss of particles in matter. If we have a beam including pions, muons and electrons with the same momentum, electrons have a smaller energy-loss than pions and muons in the plastic scintillator. The examples of detector pulse and outputs of leading edge type discriminator are shown in Fig. 3.6. Considering the energy-loss of each particle with the same momentum around 100 MeV/c, the pulse 1, 2 and 3 in Fig. 3.6 correspond to electrons, muons and pions, respectively. Suppose we employ the leading edge trigger type discriminator with the fixed discriminator level, each particle has the different triggering time as shown in Fig. 3.6. Since these differences give a wrong time of flight, the energies of particles are overestimated.

In order to avoid the time walk, a constant fraction discriminator was used in our experiment. The constant fraction discriminator is better than a leading edge timing discriminator because it has the same triggering time, independent of the pulse amplitude and rise time. The principle[45,46] is illustrated in Fig. 3.7. The detector pulse is delayed (a) and a fraction of the undelayed pulse (b) is subtracted from it (c). The attenuated pulse exactly cancels the delayed and inverted pulse at the fraction

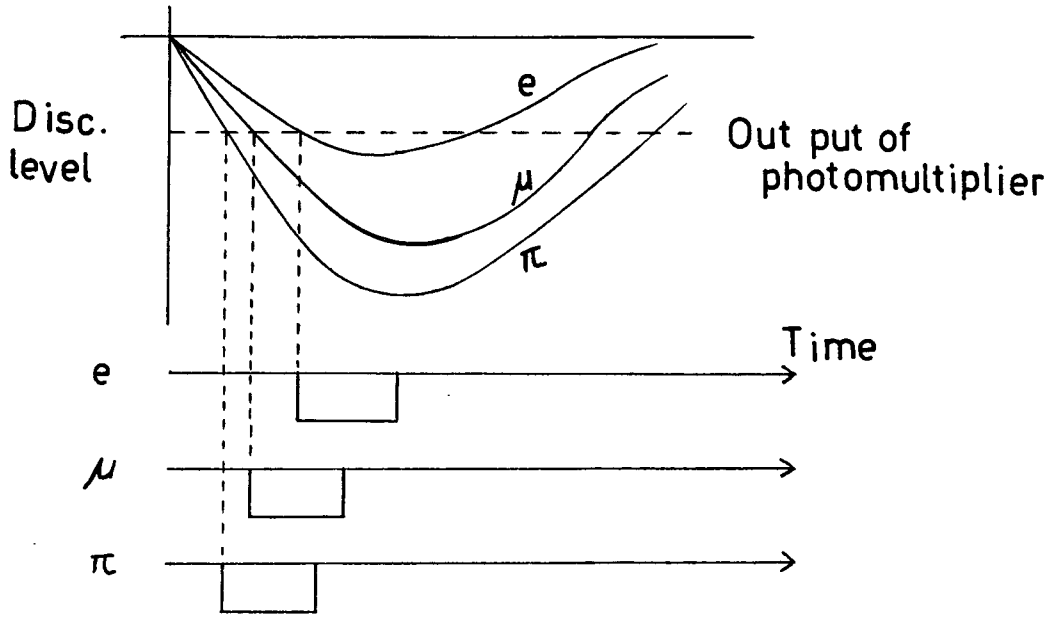

Fig. 3.6 Time-walk due to three different input pulses of electrons, muons and pions with the same momentum. Since the discriminator level of a leading edge type is fixed,the outputs shift in time spectrum.

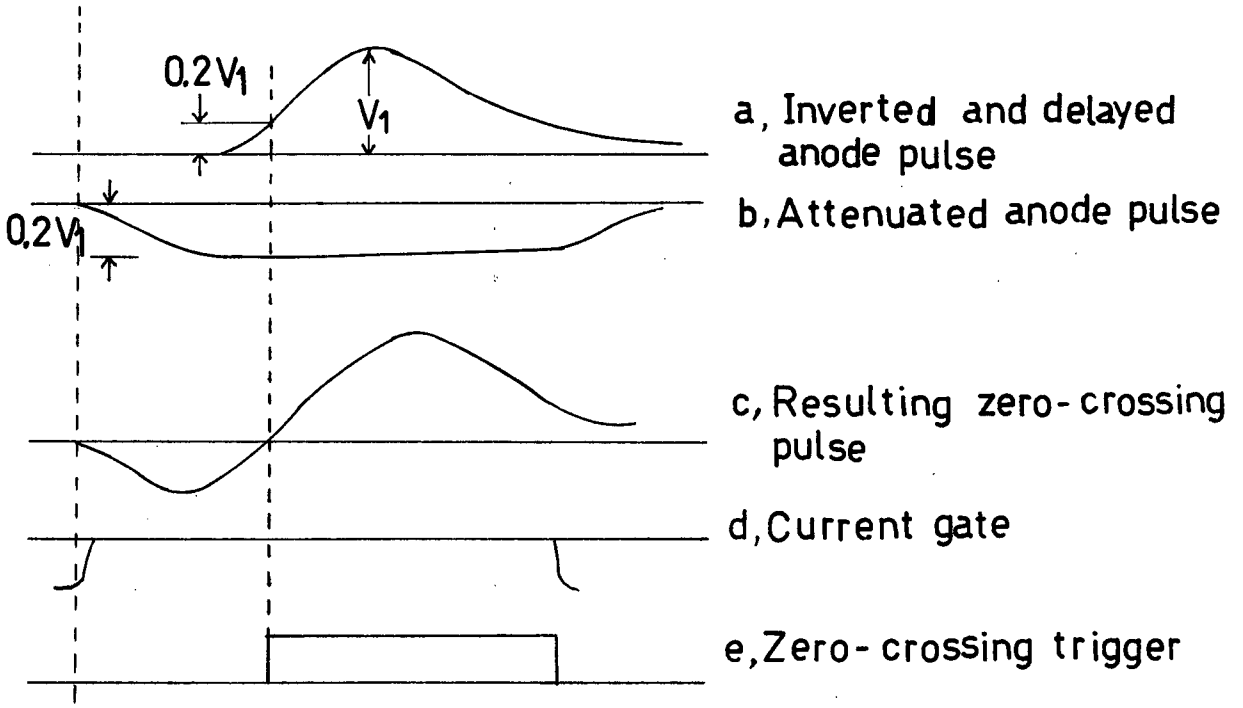

Fig. 3.7 Constant fraction of height pick-off.[45,46]

phase point on the delayed pulse.

The time of flight experiment was done at the F-3 focussing position with 50 MeV pions in order to see the effect of the time walk of a discriminator. The constant fraction discriminator (ORTEC 463) and the LRS leading edge type discriminator were employed. The results are shown in table 3.4. It is apparent that the energy of LRS discriminator gives higher energy than that of the C.F. discriminator. From the time-delay spectrum of the MCA, there is 1.0 nsec time difference between LRS and C.F. discriminator in the time of flight of the pion from the T2 to the counter. In the case of muon, this difference is about 0.8 nsec. Since the energy-loss of 30 MeV pion in the plastic scintillator (0.76 MeV) is larger than that of 50 MeV pion (0.56 MeV), the time difference for 30 MeV pion increases to 2.0 nsec.

In order to define the meson velocity by the time of flight method, we have to know the peak position of the pions and electrons on the time-delay spectrum. As seen in Fig. 4.1, the height of the electron peak comes down as the energy of pion increases. Since the contamination of electron is increased by using the target with a large atomic number, we compare the energy difference between the beryllium target and copper target. The results are shown in table 3.1. Though the height of the electron peak in case of copper is almost twice as high as that in case of beryllium, we do not detect any difference in the relative

		COPPER TARGET		BERYLLIUM TARGET	
		LRS	C.F.	LRS	C.F.
π	K.E. (MeV)	54.67 ± 2.3	51.51 ± 1.91	55.22 ± 2.31	50.93 ± 1.94
	MOMENTUM (MeV/c)	135.3 ± 3.3	130.7 ± 2.8	136.1 ± 3.3	129.8 ± 2.9
	BETA	0.695 ± 0.008	0.682 ± 0.008	0.697 ± 0.009	0.680 ± 0.008
	TIME* (nsec)	57.13 ± 0.54	58.18 ± 0.45	56.97 ± 0.53	58.39 ± 0.45
μ	K.E. (MeV)	63.91 ± 3.8	59.91 ± 3.1	62.79 ± 3.6	59.33 ± 3.0
	MOMENTUM (MeV/c)	132.8 ±4.8	127.6 ± 4.0	131.4 ± 4.6	126.9 ± 3.9
	BETA	0.782 ± 0.01	0.769 ± 0.01	0.778 ± 0.01	0.767 ± 0.01
	TIME* (nsec)	50.80 ± 0.58	51.61 ± 0.50	51.02 ± 0.56	51.74 ± 0.48

* Time of flight between the pion production target (T_2) and counter.

Table 3.3 The energies of pions and muons are measured by the time of flight method. In order to check the systematic error, two types of discriminators are employed, LRS (leading edge) and C.F. (constant fraction), and two kinds of targets, copper and beryllium.

positions of the electron and pion peaks. Thus, there is no difference in the energy determination between the targets.

IV Results and Discussion

The measurements of the time of flight and range were made on F-3. We chose four different energies, 30, 40, 50 and 60 MeV for the case of aluminum absorber and two energies, 30 and 50 MeV with the copper absorbers. The magnet currents for each energy are shown in table 4-1.

A Time of Flight

The time of flight spectra of four energies are shown in Fig. 4.1. The experimental electronics and principle of the time of flight have been discussed in the last chapter. We can see two pion peaks on the spectrum and also muon and electron peaks except for the 60 MeV case. The separation of two pion peaks corresponds to the R.F. period of 43.40 nsec. Knowing the distance from the pion production target to the counter, (8.50 ± 0.05 m), we can obtain the pion energy. In the energy calculation, we assume that the electron velocity is the velocity of light, because of its large momentum. This assumption gives negligible effect to the energy calculation of pion. For example, electrons contained in the beam with 97 MeV/c, in which pions have a K.E. of 30 MeV, have a velocity of 0.99999 ($=\beta$). Fig. 4.1 shows that the beam consists mainly of pions with a few muons and electrons. Though we can expect muons from the decay of pions, most of the muons in the muon peak come from the production target. Because the peak has a velocity corresponding to muons with the momentum determined by the channel.

ENERGY, MeV	29.4	39.5	50.5	59.0
MOMENTUM, MeV/c	95.4	112.3	129.2	141.2
MAGNET, Amp B_1	247.4	291.2	335.0	366.0
B_2	252.6	297.0	342.0	373.0
Q_1	192.0	226.0	260.0	284.0
Q_2	159.5	187.8	216.0	235.0
Q_3	129.2	152.0	175.0	191.0
Q_4	169.1	199.0	229.0	250.0
Q_5	178.7	210.0	242.0	265.0

Table 4.1 Magnet currents for the time of flight and range measurements.

MAGNET ENERGY		TIME OF FLIGHT	RANGE OF Al	RANGE OF Cu
29.4	PION	30.9 ± 0.9	29.8 ± 0.8	30.1 ± 1.2
	MUON	37.4 ± 1.6	36.1 ± 1.3	36.4 ± 1.1
39.5		41.5 ± 1.5	39.6 ± 1.1	
50.5		52.4 ± 2.2	49.7 ± 1.1*	50.3 ± 1.8
			50.1 ± 1.4**	
59.0		60.6 ± 2.9	58.6 ± 1.0*	
			59.0 ± 1.4**	

* Fitted with the Gaussian distribution.
** Fitted with the extreme value distribution.

Table 4.2 The energy in MeV obtained by the time of flight and range measurements.

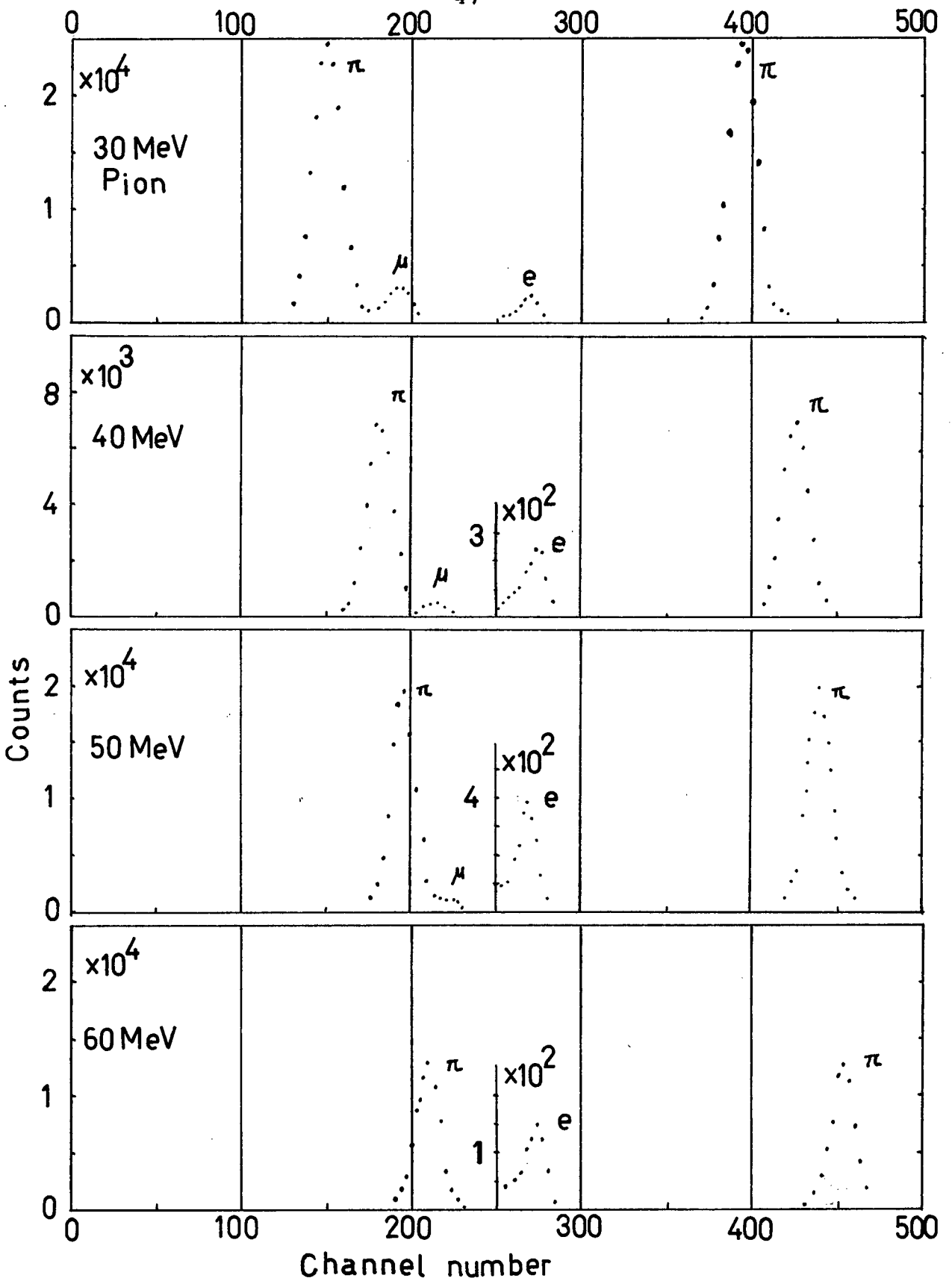

Fig. 4.1 R.F.-referenced time of flight spectrum for 30,40,50 and 60 MeV of pion energies.

The decay muons would appear between the muon and electron peak but the experimental spectra do not show clear evidence for such muons.

The pion peak has a time spread. In our time of flight measurements, the R.F. signal of the accelerator is used as the stop pulse against the start pulse of the second counter. The proton beam at the pion production target has a bunch of about 4 nsec. This is the principal contributor to the time spread as measured in our method. The peak width at half maximum is 3.6 nsec and nearly equals the proton beam time spread. Also the energy resolution ($\frac{\Delta E}{E}$) and momentum resolution ($\frac{\Delta P}{P}$) of the 30 MeV pion are 8.2 % and 4.5 % at FWHM, respectively.

In order to calculate the peak position in the time of flight spectrum, the data points are fitted with a Gaussian distribution.[47] The value of the measured position is written as $\bar{X} \pm \alpha$ where $\alpha = \frac{\sigma}{\sqrt{n}}$ is the standard error of the mean and n is the number of data points. The curve fitting program is written by using the LQF subroutine which is one of the least squares fitting program in the UBC computer library program.[48] The results are shown in table 4.2. The energies have been defined with a deviation of 3 to 5 %.

B Range Measurement

The range curves for Al and Cu are shown in Fig. 4.2 and 4.3, respectively. The energies obtained from ranges are shown in table 4.2. The experimental data are fitted with a Gaussian distribution as discussed in the last section. The curves of the Gaussian distribution and the data are illustrated in Fig. 4.2 and 4.3 by a solid line and dots, respectively.

In order to calculate the energy of pion, we have to know the thickness and content of the absorber in detail. The thicknesses of the metal of the degrader are given by the peak position of the fitted curve with the Gaussian distribution. Elements contained in the absorber are shown in table 2.2. Since, in both the aluminum and copper absorber, 99.5 % of the constituents can be considered as elements with similar atomic numbers, the effects from the different elements can be neglected in the range calculation. We have to count the thickness of plastic scintillators and also the windows which keep a vacuum in the M9 channel. The thicknesses of plastic scintillator are shown in table 2.1. Each plastic is covered by black vinyl tape, with a thickness of 180 microns, in order to keep out light. The vacuum window is made of mylar of 0.25 mm thickness. The density of plastic scintillator (NE 102A) is 1.032 g/cm^3 and its total thickness including the first, second and third counter is 0.983 ± 0.1 g/cm^2. Assuming the density of the black vinyl tape and mylar as 1.0 g/cm^3, we get 0.037 g/cm^2

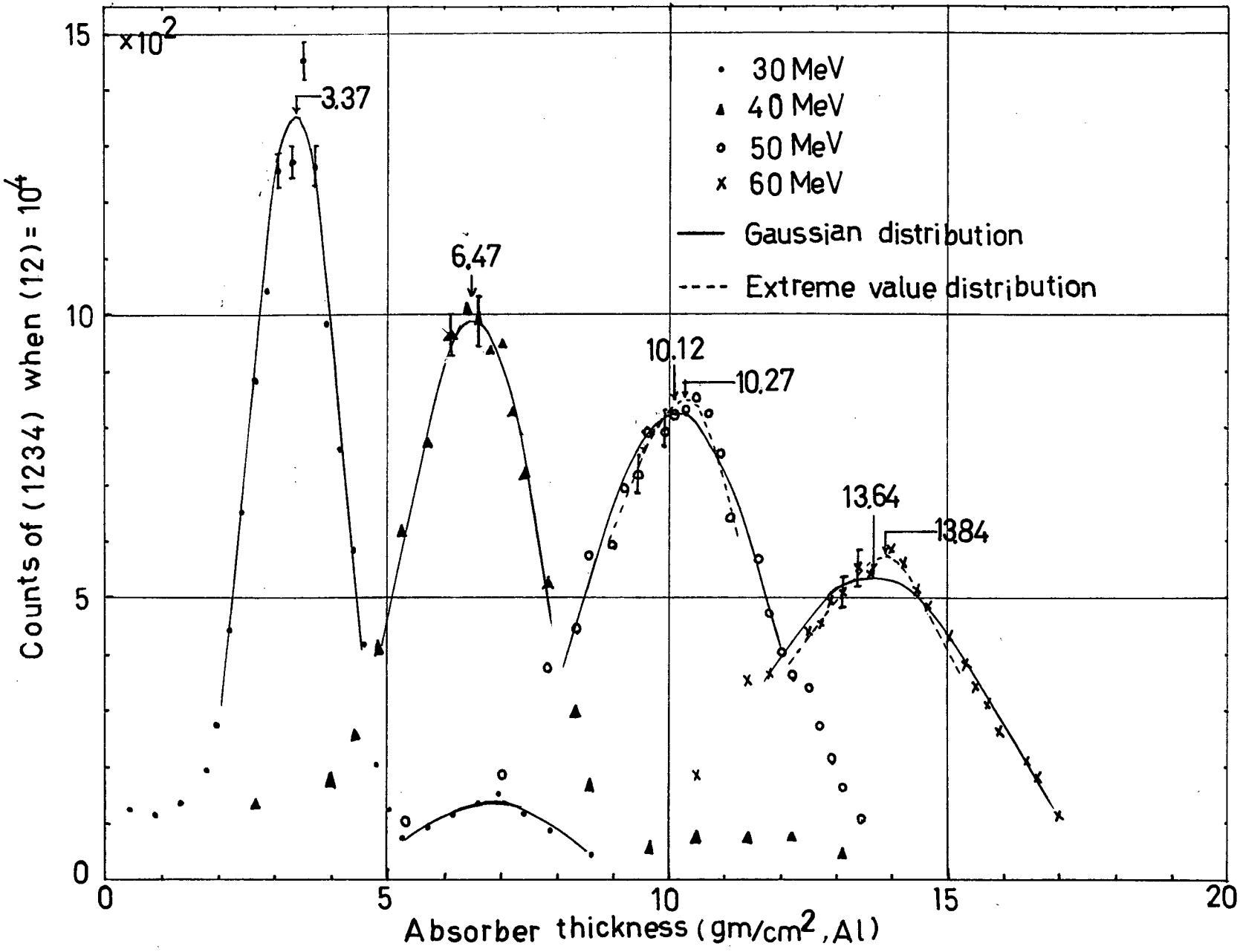

Fig. 4.2 The range curves of pion in aluminum(pion energies,30,40,50 and 60 MeV)

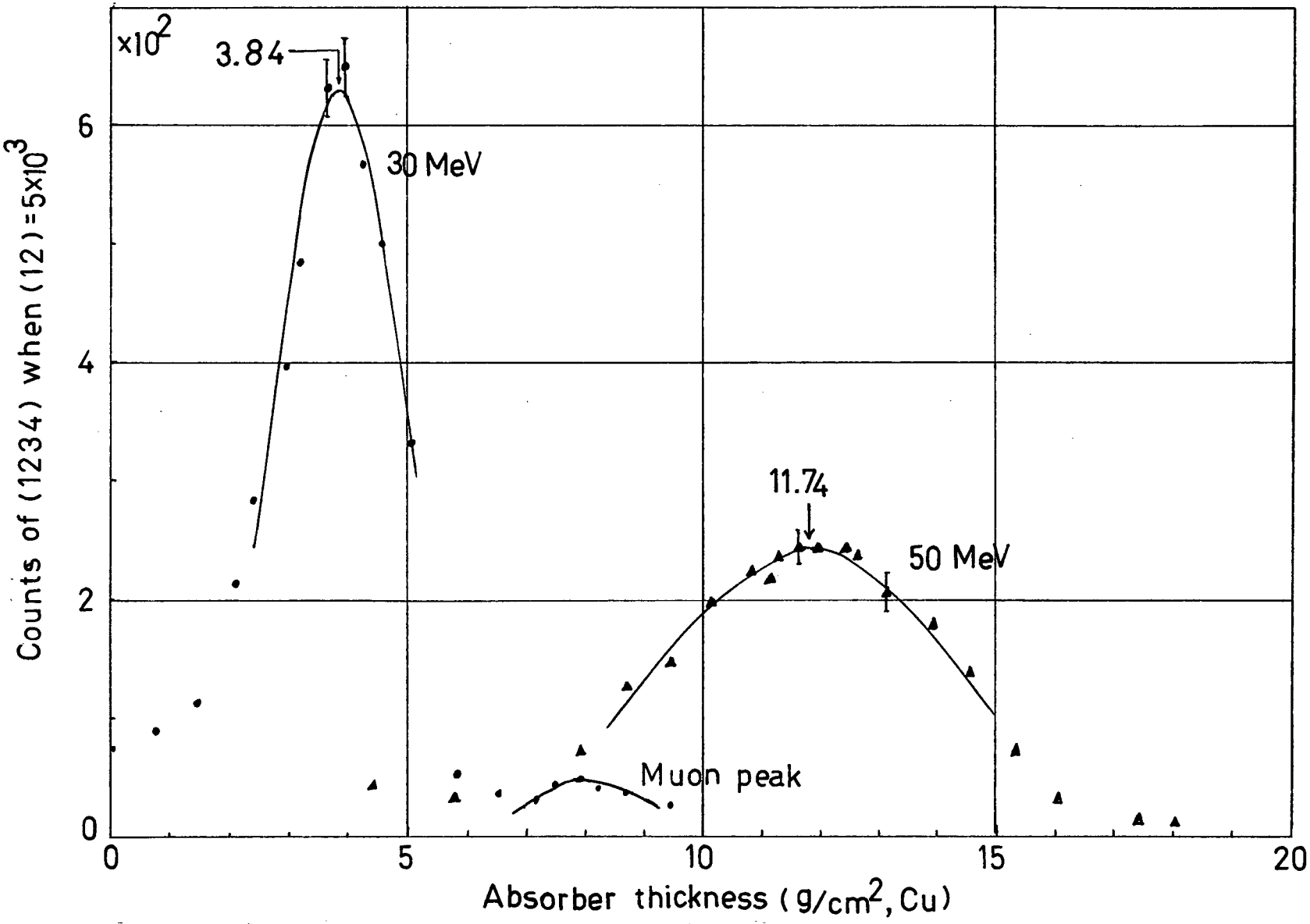

Fig. 4.3 The range curves of pion in copper(pion energies,30 and 50 MeV).

for these absorbers. The error caused from the assumption of the density as 1.0 g/cm^2 might be negligible in comparison with the total thickness due to the small number. Thus, the thickness of absorber besides the metal is 1.02±0.1 g/cm^2.

The ratio of the number H versus C is 1.104 in the plastic scintillator. The stopping powers of $CH_{1.104}$ are calculated by using the numbers of stopping power in the reference 16 and show in table 4.3. Assuming that the thickness of 1.02 g/cm^2 obtained above is made of $CH_{1.1}$, we can calculate the equivalent thickness of $CH_{1.1}$ for the aluminum and copper range curves (table 4.3).

Since the M9 channel has a vacuum of less than 0.05 mm Hg, we can neglect the slowing down of charged particles by air inside the channel. After emerging from the vacuum pipe, the charged particles still have to go through air of 1 m or so, which has a density of 1.29 mg/cm^3. This contributes to the slowing down of charged particles. The effect corresponds to 0.15 g/cm^2 in aluminum range and 0.17 g/cm^2 in copper range.

For 50 and 60 MeV range curves of aluminum, the data are also fitted with the extreme value distribution,[49] because χ^2-test for the curve fitting with the Gaussian distribution is worse than that of the extreme value distribution. The probability density function is given by

$$P(R) = \frac{1}{\sigma} \exp\left\{-\frac{\mu - R}{\sigma} - \exp\left(-\frac{\mu - R}{\sigma}\right)\right\} \qquad (4.1)$$

PION ENERGY	STOPPING POWER OF $CH_{1.1}$	EQUIVALENT RANGE OF $CH_{1.1}$		RANGE OBTAINED FROM RANGE CURVES		TOTAL RANGE**	
		Al	Cu	Al	Cu	Al	Cu
MeV	Mev-cm^2/g	g/cm^2	g/cm^2	g/cm^2	g/cm^2	g/cm^2	g/cm^2
30	4.443	1.29±0.10	1.49±0.10	3.40±0.23	3.84±0.37	4.95±0.23	5.86±0.37
40	3.723	1.28±0.10		6.47±0.37		8.01±0.37	
50	3.230	1.26±0.10	1.44±0.10	10.12±0.41 10.27±0.55*	11.74±0.75	11.64±0.41 11.79±0.55*	13.71±0.75
60	2.945	1.25±0.10		13.64±0.43 13.84±0.60*		15.15±0.43 15.35±0.60*	

* Range curves are fitted with the Extreme value distribution.

** The thickness of stopping plate behind the third counter are considered.

Table 4.3 The detail of range calculation.

The curves fitted with two distributions are shown in Fig. 4.2. It is clear that the extreme value distribution gives good fitting around the peak and the peak position shifts a little from the Gaussian case. The energies defined by two distributions are shown in table 4.2.

The aluminum plate with 0.220 g/cm^2 thickness was installed to stop pions between the third and fourth counter. A half of the thickness of the plate is considered to contribute to the range. For the copper range curves, we employed the copper plate with 0.728 g/cm^2 thickness behind the third counter. The total ranges shown in table 4.3 are given by the summation of ranges in aluminum (or copper), $CH_{1.1}$ and air. In order to obtain the energy of the pions from the range, the range-energy table of reference 16 is used, and the results are shown in table 4.2. Thus, the range curves give the pion energies within an error of $\pm$ 3 %.

C The Energy Straggling and Inherent Energy Spread of the Beam

The straggling parameter S is discussed in the section 3-A. From Fig. 3.1, the value of S can be obtained and is about 0.59 g/cm^2 in aluminum range. It is difficult to get the exact value of the straggling parameter because the beam contains pions, muons and electrons, the R-axis for the pions can not be defined easily. The straggling parameter is also given by $S=\sqrt{\frac{\pi}{2}}\cdot\alpha$, where α is given by Eq. 3.1 which is employed to fit the differential curve. From the calculation of curve fitting, α =0.55 g/cm^2, then S=0.69 g/cm^2. This is close to the number obtained approximately in Fig. 3.1. The difference between the two values of S may come from the uncertainty in choosing the R-axis.

The straggling of the range of charged particles due to the fluctuations of the ionization process is calculated theoretically by Sternheimer.[50] For the case of 30 MeV pions, the straggling parameter in aluminum is equal to 0.19 g/cm^2. The difference between the straggling of range obtained from the experiment and the theoretical straggling parameter mentioned above must be mainly attributed to the energy spread of the pion beam. Thus, the energy spread of the pions, $\sqrt{\langle (R - R_0)^2 \rangle}$, is equal to 0.53 g/cm^2. The fluctuation in range and in energy-loss is related.[34] For a small thickness dR and a small energy-loss dE, $(\Delta E^2)_{dR} = (\frac{dE}{dR})^2 (\Delta R^2)_{dE}$ where $(\Delta E^2)_{dR} = \langle (E-E_0)^2 \rangle$ and $(\Delta R^2)_{dE} = \langle (R-R_0)^2 \rangle$. According to this relation, the energy spread

of pion beam, $\sqrt{\langle (E-E_0)^2 \rangle}$ yields 1.9 MeV, id, $\Delta E/E=6.3$ % ($\Delta p/p=3.2$ %) for the 30 MeV of the pion beam. These values are smaller than the values obtained by the time of flight spectrum.

D Conclusion

The various systematic effects limit the accuracy of the energy determination. We discussed the time walk of the leading edge type and constant fraction discriminator in the last chapter. Then, we could reduce the time walk by using the constant fraction discriminator. In the time of flight measurement, the time walk of the discriminator is the most serious systematic error in the energy determination. The specification[51] of the constant fracion discriminator claims that the walk is less than 0.51 nsec. If there is small time walk such as 0.1 nsec, the energy determined by the time of flight will be reduced by 0.2 (0.6) MeV for the 30 (60) MeV pion. In the energy calculation by the range method, there is the uncertainty in the range-energy table.[16] We can expect that it is better than 0.5 %.

It has been shown that there are three independent methods to determine the pion energy. The calculated magnetic currents of the M9 pion channel choose the particles with the same momentum but different energy. The time of flight and range methods actually work as a calibration of pion energy defined by the magnets of the M9 channel. In this work, we have shown that three independent methods for measuring pion energies are consistant with one another within the statistical error and pion energies can now be measured with confidence to an accuracy 2 % by range and 5 % by the time of flight method.

We can improve the accuracy of the time of flight

measurement by using a stop signal from a counter instead of the R.F. signal or by using a chopped beam with a sharp bunch. In the range-energy determination one might be able to improve the geometry of the four counters somewhat.

references:

1 W.H. Barkas and S. von Friesen, Nuovo Cimento 19, 41 (1961)

2 U.P. Zrelov and G.D. Stoletov, Soviet Physics JETP 9, 461 (1959)

3 R. Mather and E. Segre, Phys. Rev. 84, 191 (1951)

4 C.J. Bakker and E. Segre, Phys. Rev. 81, 489 (1951)

5 H. Bichsel, R.F. Mozley and W.A. Aron, Phys. Rev. 105, 1788 (1957)

6 E.A. Uehling, Nuclear Science Series 29 (1960)

7 T.D. Lagerlund, M. Blecher, K. Gotow, D. Jenkins and W.C. Lam, Nucl. Instr. and Meth. 128, 525 (1975)

8 N. Bohr, Phil. Mag. 25, 10 (1913)

9 H. Bethe, Ann. Phys. 7-5, 325 (1930)

10 M.S. Livingstone and H.A. Bethe, Rev. Modern Phys. 9, 261 (1937)

11 A.E. Taylor, Repts. Prog. in Phys. 15, 49 (1952)

12 S.K. Allison and S.D. Warshaw, Rev. Mod. Phys. 25, 779 (1953)

13 E.A. Uehling, Ann. Rev. Nucl. Sci., 4, 315 (1954)

14 W. Wahling, Encyclopedia of Physics, 3410, 193 (1958)

15 U. Fano, Ann. Rev. Nucl. Sci., 13, 1 (1963)

16 C. Serre, Cern 67-5 (1967)

17 H. Bichsel, American Institute Handbook, 8, 142 (1971)

18 H.H. Heckman and P.J. Lindstorm, Phys. Rev. Letters 22, 871 (1969)

19 J.D. Jackson and R.L. McCarthy, Phys. Rev. B, 6, 4131 (1972)

20 M. Inokuti, Rev. Mod. Phys. 43, 297 (1971)

21 D.I. Porat, IEEE Transaction on Nuclear Science NS-20, 36 (1973)

22 H.B. Mak, H.B. Jensen and C.A. Barnes, Nucl. Inst. and Meth. 109, 529 (1973)

23 J.H. Manley and M.J. Jakobson, Rev. Sci. Instr. 25, 368 (1954)

24 J.L. Romero, H. Massmann, F.P. Brady and J. Zamudio, Nucl. Instr. and Meth. 100, 551 (1972)

25 H. Bruckmann, E.L. Haase, W. Kluge and L. Schanzler, Nucl. Instr. and Meth. 67, 29 (1961)

26 A.J. Stevens, D.M. Schwartz, C.J. Ruch, K. Reibel and T.A. Romanowsk, Nucl. Instr. and Meth. 97, 207 (1971)

27 J.H. Neiler and W.M. Good, Fast Neutron Physics (IV.A) (1960) Interscience Publishers, Inc., New York

28 A.F. Elwyn, H.H. Landon, S. Oleksa and S.N. Glasoe, Phys. Rev. 112, 1200 (1958)

29 F.P. Brady, W.J. Knox and S.W. Johnson, Nucl. Instr. and Meth. 89, 309 (1970)

30 M.D. Cooper, LA-5529-MS (1974)

31 SIN Jahresbericht p70 (1974), pB14 (1975)

32 TRIUMF ANNUAL REPORT (1975)

33 E. Fermi, Nuclear Physics, The Univ. of Chicago Press (1950)

34 E. Segre, Nuclei and Particle, Benjamin (1964)

35 P. Marmier and E. Sheldon, Nuclei and Particles, Academic

Press (1970)

36 W.H. Barkas, Nuovo Cim., 8, 201 (1958)
Phys. Rev., 117, 544 (1960)
UCRL No 9420 (1960)
Nuovo Cim. Suppl. 19, 41 (1961)

37 W.O. Lock and D.F. Measday, Intermediate Energy Nuclear Physics Methuen (1970) p221

38 P.A. Reeve, File of TRIUMF, June 4, 1975

39 D. Bryman, M9 book used for M9 channel in TRIUMF

40 D.F. Measday, M.R. Menard and J.E. Spuller, Kinematics Handbook

41 J.E. Spuller, Private communication

42 Nuclear Enterprises Inc. (NEI), "Plastic Scintillators"

43 R.M. Sternheimer, Method of Experimental Physics 5-A, chapter 1

44 P.W. Nicholson, Nuclear Electronics, John Wiley & Sons

45 D.A. Gedcke and W.J. McDonald, Nucl. Instr. and Meth. 55, 377 (1967)

46 D.A. Gedcke and W.J. McDonald, Nucl. Instr. and Meth. 58, 253 (1968)

47 J. Topping, Errors of observation and their treatment, The Institute of Physics and Physical Society

48 U.B.C. computing center, U.B.C. curve fitting program

49 W.T. Eadie, D. Drijard, F.E. James, M. Roos and B. Sudoulet Statistical Methods in Experimental Physics, (NORTH HOLLAND, 1971)

50 R.M. Sternheimer, Phys. Rev. 117, 485 (1960)

51 ORTEC, ORTEC 463 Constant Fraction Discriminator